ECS | The Electrochemical Society
Advancing solid state & electrochemical science & technology

Polyaniline Electrode Activation in Li Cells

View the article online for updates and enhancements.

CrossMark

Polyaniline Electrode Activation in Li Cells

Michael Charlton,[1] T. D. Hatchard,[1] and M. N. Obrovac[1,2,*,z]

[1]*Department of Chemistry, Dalhousie University, Halifax NS, B3H 4R2 Canada*
[2]*Department of Physics and Atmospheric Science, Dalhousie University, Halifax, NSB3H 4R2, Canada*

Polyaniline (PANi) can be used as an electroactive organic cathode material in Li-cells with multiple redox states. The theoretical specific capacity of the emeraldine base (PEB) is 150 mAh g^{-1}. In this study, we show how the specific capacity of PEB$_{90-x}$CB$_x$PVDF$_{10}$ cathodes is dependent upon the mass percentage of PEB and carbon black (CB) in the potential range of 2.0–4.0 V. The capacity of PEB$_{90-x}$CB$_x$PVDF$_{10}$ cathodes is initially very low, steadily increasing during initial cycling. A constant capacity is eventually reached with continued cycling. Microscopic imaging and elemental analysis of cycled electrodes reveals how the electrode composition and morphology of PEB$_{90-x}$CB$_x$PVDF$_{10}$ cathodes plays an integral role in the magnitude of the specific capacity during the initial and steady state cycles. We propose a diffusion-limited model as an attempt to elucidate the differences in the total specific capacity among PEB$_{90-x}$CB$_x$PVDF$_{10}$ cathodes. From our findings, we propose that increasing CB content provides more ion-diffusion channels throughout the PEB$_{90-x}$CB$_x$PVDF$_{10}$ cathodes. This model is consistent with our findings in that more CB content reduces the amount of cycles required to reach steady state cycling and increases the magnitude of the specific capacity at steady state.

Electrochemically active organic species can be utilized as cathodes in Li-ion batteries. The redox chemistry of organic species is different from inorganic species. Redox reactions of an inorganic species typically involve changes in an ion's oxidation state. For an organic species, redox reactions involve the oxidation/reduction of an entire organic group.[1] Organic electrode materials are attractive candidates for sustainable and versatile energy storage devices, and possess inherent advantages over inorganic electrode materials.[1–6] Organic based materials and their functionalized derivatives are more numerous and structurally diverse than inorganic based materials. As a consequence, there exists a panoply of potential electroactive organic compounds and their derivatives.[1,2,7–11] Furthermore, organic active materials can be functionalized in order to alter and improve their electrochemical characteristics (e.g. oxidative stability).[12] On the contrary, inorganic cathode research is much more restrictive.[13–17] However, significant disadvantages and challenges must still be overcome before organic electrode materials can be utilized practically in commercial Li-ion batteries.[1]

Polyaniline (PANi) is a conductive organic polymer that can be implemented as an electroactive cathode material in Li-ion cells.[9,18,19] PANi is classified as a p-type organic electrode material.[1] A p-type organic electrode material involves a redox reaction between a neutral state and a positively charged state during charge and discharge.[1] Several of the disadvantages which organic electrode materials typically possess are not applicable to PANi. For example, non-conjugated electroactive organics suffer from low electronic conductivity. However, PANi is a conjugated amine, and is therefore electronically conductive. Another disadvantage of low molecular weight (MW) organic materials is their solubility in organic electrolytes. Since PANi is a higher mass polymer, it remains insoluble in most organic electrolytes. Furthermore, PANi is easily synthesized and can undergo multi-redox reactions, making it an attractive organic electrode material.

Figure 1 illustrates the redox states of PANi. The reversible 2-electrode oxidation of leucoemeraldine base (Fig. 1a) to emeraldine salt (PEB) (Fig. 1b) has a theoretical specific capacity of 150 mAh g^{-1}.[9,12] During this process, two anions from the electrolyte are inserted into the leucoemeraldine base. In a Li-cell, Li$^+$ from the

electrolyte would be simultaneously reduced at the anode. Therefore, during the charge of a Li-cell with a PANi cathode, the electrolyte is depleted of ions. The pernigraniline salt, Fig. 1c, is formed via the reversible 2-electron oxidation of PEB, also involving the extraction of two anions from the electrolyte, and corresponding to a theoretical specific capacity of 150 mAh g^{-1}.[12] However, such capacity cannot be realized as pernigraniline salt is unstable and irreversibly forms inactive pernigraniline base, Fig. 1d, at increasingly oxidizing potentials.

In this study, cathodes were made from the PEB form of PANi and incorporated in Li half-cells. In previous publications, PEB electrodes have been shown to have a stable capacity.[9,18–20] We have found that not to be the case. Upon closer examination of previous studies, it became clear that the PEB electrodes were cycled with a series of formation cycles, which are never described or shown. We have found that all PEB electrodes require significant formation cycles in order for stable capacity to be established. To our knowledge, this property has never been reported. In this study the formation of PEB electrodes is explored and its relation to electrode formulation.

Experimental

PEB was used as received from 3M company. Working electrodes were prepared by mixing PEB, carbon black (CB) (C-NERGY Super C 65, Imerys Graphite and Carbon), and polyvinylidene fluoride (PVDF) binder (HSV 900, Kynar) in a (90-x):x:10 mass ratio ($10 \leqslant x \leqslant 40$). The final electrodes are referred to as PEB$_{90-x}$CB$_x$PVDF$_{10}$. For each coating, *N*-methyl-2-pyrrolidone (NMP) (Sigma-Aldrich, anhydrous 99.5%) was used in an amount that was ten times the total mass of the solid materials. The slurries for PEB$_{90-x}$CB$_x$PVDF$_{10}$ cathodes were prepared in a two-step method. In the first step only the CB and PVDF were combined, with approximately 20% of the total NMP mass. These components were mixed with two 12 mm tungsten carbide balls in a Retsch PM200 rotary mill (100 rpm, 10 min). For the second step, the PEB and the remaining amount of NMP were then added to the slurry, and these components were then mixed further (100 rpm, 20 min). The mixed slurries were coated onto aluminum foil using a coating bar having a 0.102 mm gap. The coatings were dried in a solvent oven at 110 °C for 60 min. Coating adhesion to the Al current collector was relatively poor. Cathode compositions with x > 40

*Electrochemical Society Member.
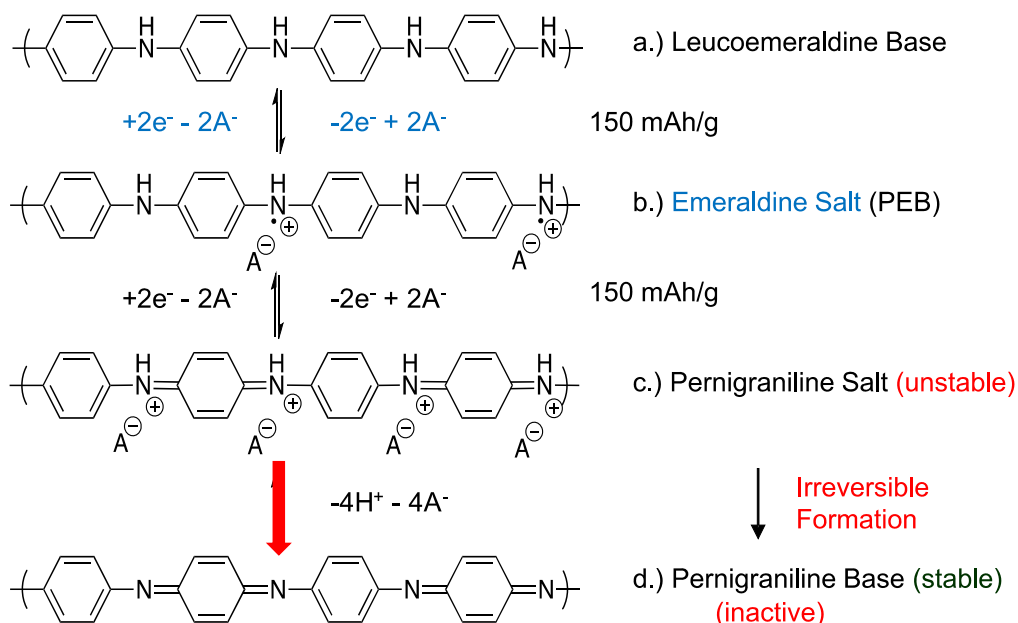zE-mail: mnobrovac@dal.ca

Figure 1. The multi-redox states of PANi. Adapted from Chen et al.[12]

were not studied, as the mechanical integrity of the coating becomes too poor at these compositions. The average loading of the cathodes was approximately 0.050 mAh cm^{-2}. CB$_{90}$PVDF$_{10}$ coatings were also prepared using a similar method.

Circular electrodes were punched from the coatings and incorporated into 2325-type coin half-cells, which were prepared in an Ar-filled glovebox. 0.125 M LiClO$_4$ (Sigma Aldrich, ⩾95%) in a solution of ethylene carbonate and diethyl carbonate (volume ratio 1:2, battery grade, all from BASF) was used as the electrolyte. Two layers of Celgard-2300 separator and one interleaving layer of BMF separator (3M company) were used as cell separators. In each half-cell, each working electrode was paired with a 2.57 cm^2 circular lithium metal foil counter electrode (thickness of 0.38 mm, 99.9%, Sigma-Aldrich) and 200 μl of electrolyte was used.

All cells were evaluated using a Maccor Series 4000 Automated Test System while the cells were thermostatically controlled at 30.0 ± 0.1 °C. The prepared cells were cycled between 2.0 V and 4.0 V at a rate of C/10. All C-rates were calculated with respect to the mass of PEB in the electrodes, assuming a theoretical capacity of 150 mAh g^{-1}. The average loading of the PEB cells studied were 0.0143 Ah g^{-1}, varying only slightly (±0.0004 Ah g^{-1}) across each PEB$_{90-x}$CB$_x$PVDF$_{10}$ cathode composition studied.

The morphology of fresh and cycled electrodes were analyzed by first cross sectioning electrodes in a cross section polisher (JEOL IB-19530) and then imaging using a scanning electron microscope (TESCAN, MIRA3) with an accelerating potential of 5 kV. The cycled electrodes were recovered in an Ar-filled glove box and rinsed with dimethyl carbonate (DMC) (battery grade from BASF) in order to remove residual salt. Air exposure was minimized through rapid transfer from an argon atmosphere to the microscope antechamber. PEB$_{70}$CB$_{20}$PVDF$_{10}$ electrodes examined via SEM and EDS analysis (Figs. 7, 8) were cycled at a rate of C/7.

Results and Discussion

Figures 2a and 2b show a backscattered electron (BSE) SEM image and a fluorine map, respectively, of a cross section of a pristine PEB$_{70}$CB$_{20}$PVDF$_{10}$ electrode. These images are typical of all electrodes made in this study. The micrograph reveals a network of bright and dark regions ∼0.2 μm in size, which may represent a dispersion of carbon black throughout the coating. Furthermore, the fluorine map in Fig. 2b illustrates that the PVDF is distributed throughout the coating. There are voids also present in the coating,

possibly from solvent loss during the drying process. These voids are present throughout the bulk of the coating, as revealed by the cross-section image and were found to be present in all PEB electrode compositions in this study.

Figure 3 shows the potential profile of a Li half-cell containing a PEB$_{70}$CB$_{20}$PVDF$_{10}$ cathode. Its reversible capacity increases with cycle number. This is typical of all the PEB$_{90-x}$CB$_x$PVDF$_{10}$ cathodes made in this study. After multiple cycles, the reversible capacity of PEB$_{90-x}$CB$_x$PVDF$_{10}$ cathodes eventually reaches an approximately constant value. Therefore, PEB$_{90-x}$CB$_x$PVDF$_{10}$ cathodes require formation cycles prior to achieving steady state cycling. This is illustrated clearly in Fig. 4, which shows the specific capacity (per gram of PEB) plotted vs cycle number for all the PEB$_{90-x}$CB$_x$PVDF$_{10}$ cathodes. The specific capacity generally increases as x increases and the number of cycles needed to reach steady state decreases with x. These trends are likely due to improved diffusion in the electrode coating by the introduction of CB, as will be discussed further below. However, the electrode with x = 40 does not follow this trend. This is likely due to the poor quality of the x = 40 electrode, as the electrodes suffered from poor adhesion and poor mechanical properties as x increased.

Figures 5a and 5b show the potential profiles and differential capacity curves of PEB$_{90-x}$CB$_x$PVDF$_{10}$ cathodes after formation cycles when the capacity reached a steady state. The highest reversible capacity achieved is about 140 mAh/(g PEB) for the PEB$_{90-x}$CB$_x$PVDF$_{10}$ cathodes with x = 30 and x = 40. This is close to the PEB theoretical capacity of 150 mAh g^{-1}. However, not all this capacity may be coming from PEB, as will be discussed below. The potential profile of the electrode with x = 10 comprises a single sloping region and suffers from a high polarization of about 250 mV. The electrodes with higher values of x have less polarization (∼130 mV). Their potential profiles consist of a sloping region in the 2 V to 2.9 V range and one in the 2.9 V to 4 V range. This can be seen more clearly in the differential capacity, where the PEB$_{80}$CB$_{10}$PVDF$_{10}$ cathode, has almost no electrochemical activity below 2.9 V, while as the carbon black content increases, there is an increasing amount of capacity in this potential range. The extra capacity below 2.9 V is apparently related to the CB content in the electrode.

Figure 6 shows the differential capacity of a charge half-cycle of a PEB$_{80}$CB$_{10}$PVDF$_{10}$ cathode and a CB$_{90}$PVDF$_{10}$ cathode. From this plot it can be seen that CB contributes capacity across the entire potential range of 2.0–4.0 V, while PEB contributes capacity in the potential range of approximately 2.9–4.0 V. However, the charge
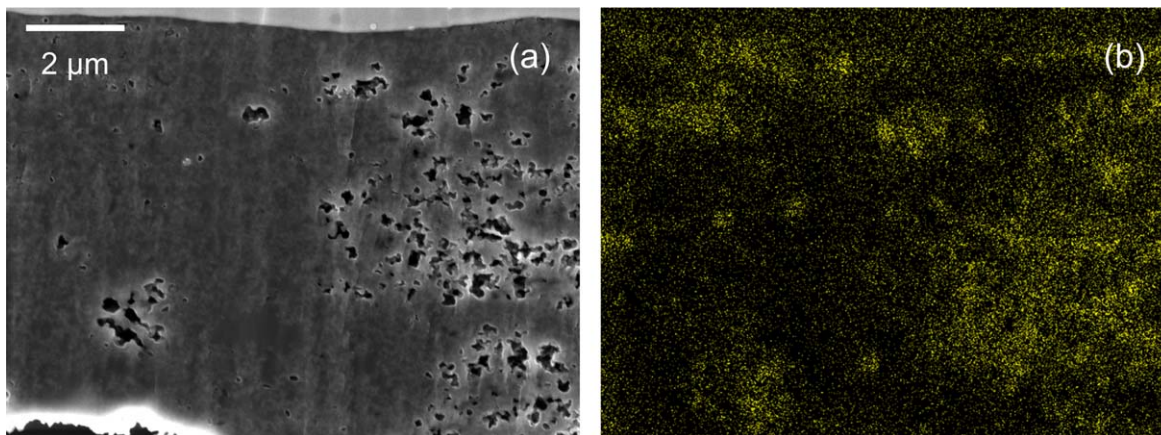
Figure 2. (a) An SEM image and (b) an EDS fluorine elemental map of a $PEB_{70}CB_{20}PVDF_{10}$ electrode before cycling.
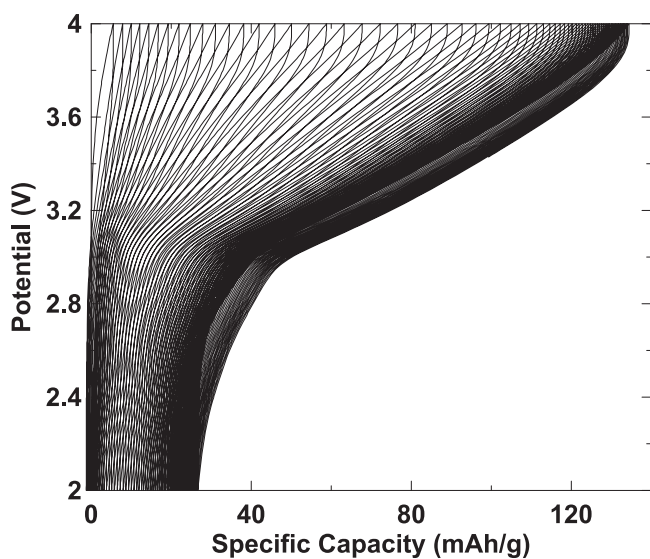

Figure 3. Potential profile of a $PEB_{70}CB_{20}PVDF_{10}$ cathode.
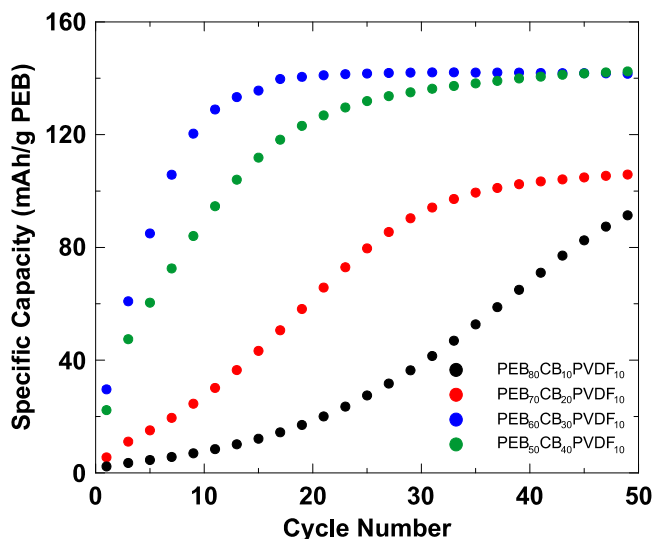

Figure 4. Specific capacity (mAh/g PEB) vs cycle number of all $PEB_{90-x}CB_xPVDF_{10}$ cathodes.

capacity of CB in this electrolyte is small (only about 10 mAh g^{-1}) compared to the capacity observed below 2.9 V. For instance, for the

CB to contribute all the capacity below 2.9 V for the $PEB_{70}CB_{20}PVDF_{10}$ cathode would correspond to a CB capacity of about 70 mAh g^{-1} or about seven times that observed for CB on its own. From these results, there seems to be synergistic effects between PEB and CB in these electrodes. That is, coatings with a low CB content have a low PEB capacity and coatings with low PEB content have a low CB capacity, while coatings with significant amounts of PEB and CB have high PEB and CB capacities. The presence of CB in the coating improves Li$^+$ diffusion in the coating, as will be shown below, which can help PEB achieve its full capacity. It is not clear, however, how the presence of PEB can result in a larger CB capacity.

Coin cells containing $PEB_{70}CB_{20}PVDF_{10}$ cathodes were constructed and cycled for 50 cycles (Sample A) and 11 cycles (Sample B). Both cells were then fully charged and held at a potential of 4.0 V. Figure 7a shows the cycling capacity, SEM images and EDS compositional maps of post-cycled electrode cross sections. The surface of the electrode that was in contact with the cell electrolyte is at the bottom edge of the figures. Since perchlorate (ClO_4^-) anions insert into the active material during charge, the presence of Cl and O in the elemental maps indicate the presence of perchlorate anions. However, Cl is a better indicator for perchlorate content than O, because of possible air exposure of the electrodes during the measurement process. It can be inferred from the relative intensity of atomic Cl that there was more perchlorate inserted into Sample A than Sample B, as expected. In Sample A, the Cl content is relatively homogeneous. However, in Sample B there are areas randomly positioned throughout the electrode in which no Cl is present. Apparently, during cycling the entire thickness of the electrode can be accessed by perchlorate, but not in a homogeneous way. The electrode contains a number of irregularly-shaped voids that are typical of those seen in the electrode prior to cycling (Fig. 2). In addition, a number of distinct linear cracks and fissures are present in the electrode, parallel to the coating direction that were not present prior to cycling. Therefore, these cracks apparently are formed as a result of the cycling process, while the irregularly-shaped voids are unchanged during cycling. The crack concentration was largest in Sample A. These cracks likely arise from volume expansion during ClO_4^- insertion. The $PEB_{60}CB_{30}PVDF_{10}$ electrode showed similar behavior. Figure S1 (available online at stacks.iop.org/JES/167/080501/mmedia) shows higher magnification cross-section images of a $PEB_{60}CB_{30}PVDF_{10}$ electrode before and after 50 cycles, where severe cracks are also observed to appear.

Considering the above results, we suggest that the carbon black added to the electrode provides electronic and ionic conducting pathways throughout the electrode. This model is illustrated in Fig. 8. $PEB_{90-x}CB_xPVDF_{10}$ electrode coatings comprise carbon black dispersed throughout the coating. According to our model, during charge ClO_4^- ions can diffuse into the electrode easiest
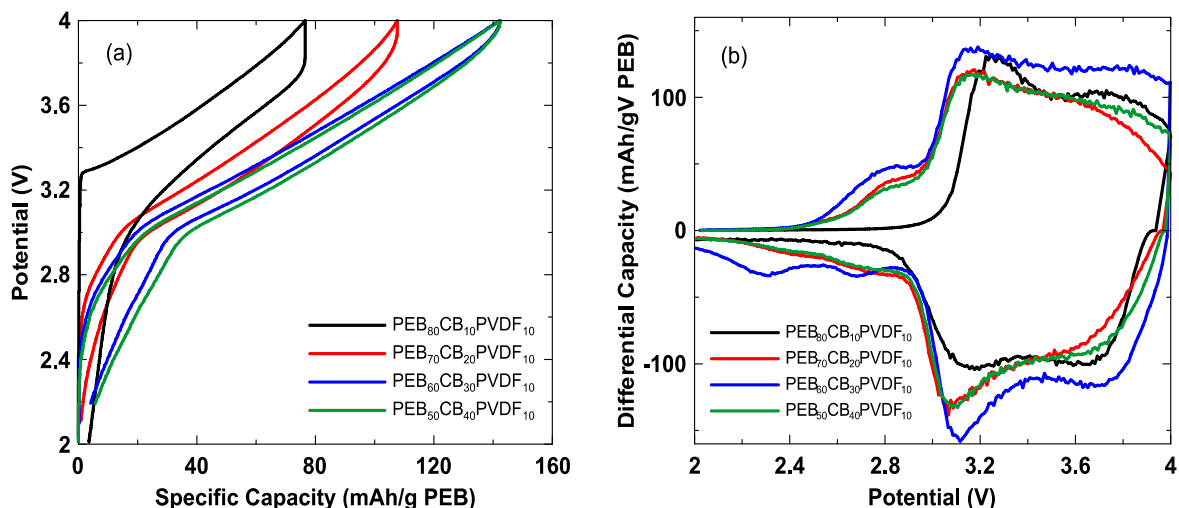
Figure 5. (a) Potential profiles (mAh/g PEB) at steady state cycling of all $PEB_{90-x}CB_xPVDF_{10}$ cathodes studied and (b) Differential capacity (mAh/gV PEB) curves of all $PEB_{90-x}CB_xPVDF_{10}$ cathodes studied.
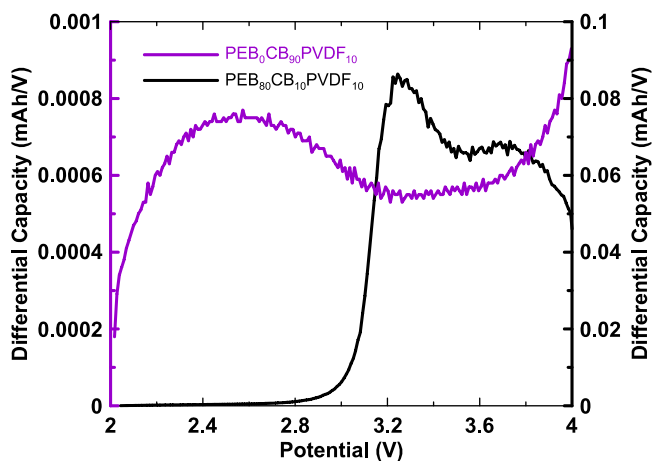

Figure 6. Differential capacity curves of $CB_{90}PVDF_{10}$ and $PEB_{80}CB_{10}PVDF_{10}$ cathodes.

through the carbon black, while diffusion in PEB is slow. Therefore, ClO_4^- insertion into PEB only starts near areas rich in carbon black. This results in electrode expansion, which creates fissures in the electrode, improving diffusion further, until eventually all of the electrode coating is accessible towards ClO_4^- insertion. In order to further confirm this model, a cell was constructed with a $PEB_{70}CB_{20}PVDF_{10}$ cathode, charged to 4.0 V and was held at this potential for 15 d. This time interval is approximately the total amount of charge time before steady state cycling is reached when cycling this electrode at a rate of C/10. After this hold at constant potential, the electrode was cycled between 2.0–4.0 V at a rate of C/10. Figure 9 compares the cycling data of this cell with that of a $PEB_{70}CB_{20}PVDF_{10}$ cathode that has been cycled at a C/10 rate without this potential hold step. After being held at a potential of 4.0 V for 15 d, upon cycling, the $PEB_{70}CB_{20}PVDF_{10}$ cathode starts with an increased capacity relative to standard cycling. A $PEB_{90-x}CB_xPVDF_{10}$ cathode held at full charge for an extended period of time appears to provide an opportunity for perchlorate
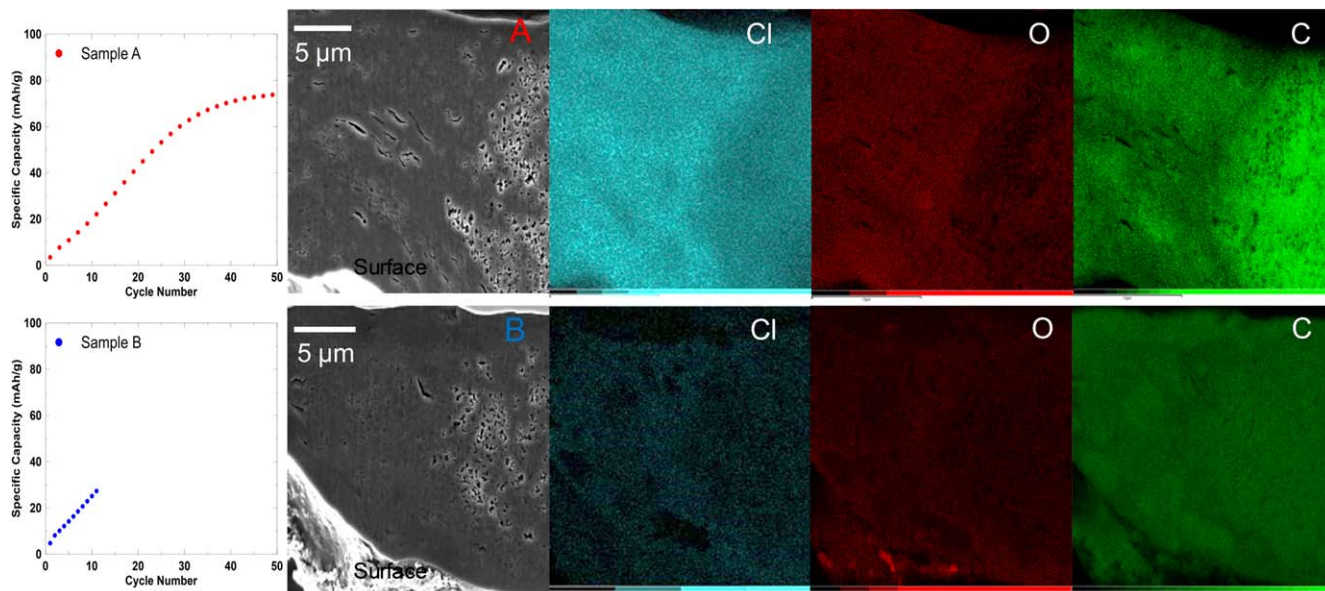

Figure 7. EDS mapping and SEM imaging of $PEB_{70}CB_{20}PVDF_{10}$ cathodes cycled for 50 cycles (a) and 11 cycles (b).

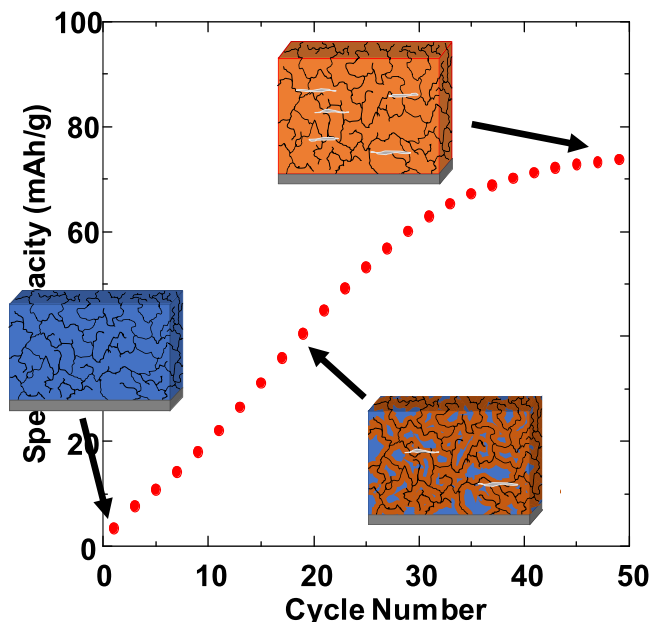**Figure 8.** Model showing the evolution of $PEB_{90-x}CB_xPVDF_{10}$ cathodes during cycling. blue: PEB, black: CB, grey: current collector, orange: charged PEB, white: fissures formed by volume expansion.
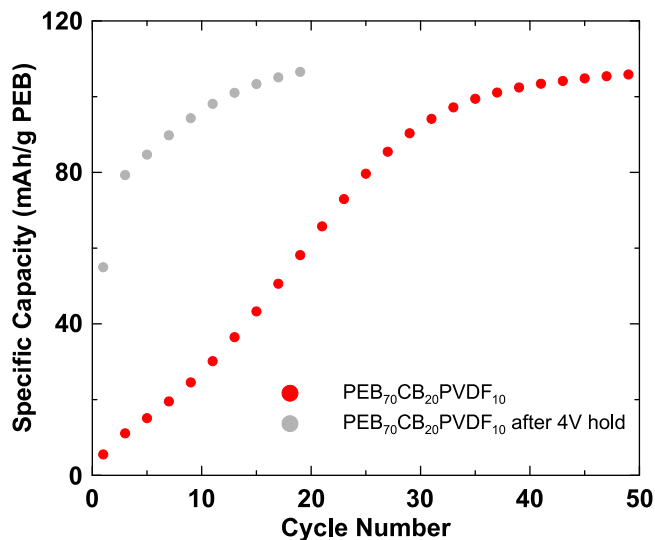

Figure 9. Specific capacity (mAh/g PEB) vs cycle number of $PEB_{70}CB_{20}PVDF_{10}$. One electrode has been cycled under standard conditions. The other has been held at 4 V for 15 h prior to cycling.

anions to access a significant amount of active sites. This is consistent with the diffusion limited model we propose above.

Conclusions

The electrochemistry of $PEB_{90-x}CB_xPVDF_{10}$ cathodes towards perchlorate insertion was investigated in the 2.0–4.0 V potential range. These electrodes were found to have a low initial reversible capacity that eventually increased to a steady-state capacity after 10 −50 cycles. The addition of carbon black both increased the steady-state capacity and reduced the number of cycles needed to attain steady-state. Both CB and PEB were found to significantly contribute to electrode capacity in a synergistic way. The low initial capacity was found to be caused by a diffusion limited process, where the addition of CB was found to significantly improve diffusion. A model was proposed in which CB provides diffusion paths for ClO_4^- throughout the electrode, while diffusion into PEB regions of the electrode is slow. This model agrees well with elemental maps that show inhomogeneous ClO_4^- distribution throughout charged electrodes at the initial stages of cycling.

ORCID

M. N. Obrovac https://orcid.org/0000-0001-5509-3185

References

1. Z. Song and H. Zhou, *Energy & Enviro. Sci.*, **6**, 2280 (2013).
2. K. Oyaizu and H. Nishide, *Adv. Mater.*, **21**, 2339 (2009).
3. H. Senoh, M. Yao, H. Sakaebe, K. Yasuda, and Z. Siroma, *Electrochim. Acta*, **56**, 10145 (2011).
4. P. Poizot and F. Dolhelm, *Energy Environ. Sci.*, **4**, 2003 (2011).
5. G. Milczarek and O. Inganas, *Science*, **335**, 1468 (2012).
6. G. Li, C. Li, G. R. Li, S. H. Ye, and X. P. Gao, *Adv. Energy Mater.*, **2**, 1238 (2012).
7. P. J Nigrey, D MacInnes, D. P Nairns, and A. G MacDiarmid, *J. Electrochem. Soc.*, **128**, 1651 (1981).
8. S. R. Deng, L. B. Kong, G. Q. Hu, T. Wu, D. Li, Y. H. Zhou, and Z. Y. Li, *Electrochim. Acta*, **51**, 2589 (2006).
9. W. Huang, B. D. Humphrey, and A. G. MacDiarmid, *J. Chem. Soc., Faraday Trans.*, **82**, 2385–2400 (1986).
10. K. Kaneto, S. Ura, P. Film, K. Kaneto, and G. Ishii, *Japan. J. Appl. Phys.*, **22**, L567 (1983).
11. L. Zhan, Z. Song, J. Zhang, J. Tang, H. Zhan, Y. Zhou, and C. Zhan, *Electrochim. Acta*, **53**, 8319 (2008).
12. Y. Chen and S. Manzhos, *J. Power Sources*, **336**, 126 (2016).
13. M. Li, J. Lu, Z. Chen, and K. Amine, *Adv. Mater.*, **30**, 1800561 (2018).
14. J. W. Fergus, *Journal of power sources*, **195**, 939–954 (2010).
15. N. Nitta, F. Wu, J. T. Lee, and G. Yushin, *Mater. Today*, **18**, 252 (2015).
16. G. E. Blomgren, *J. Electrochem. Soc.*, **164**, A5019 (2017).
17. F. Lin, I. M. Markus, D. Nordlund, T. C. Weng, M. D. Asta, H. L. Xin, and M. M. Doeff, *Nat. Commun.*, **5**, 3529 (2014).
18. H. Wang, J. Lin, and Z. X. Shen, *J. Sci. Adv. Mater. Devices*, **1**, 225 (2016).
19. L. Yang, W. Qui, and Q. Liu, *Solid State Ionics*, **86**, 819 (1996).
20. Y. Lan-Sheng, S. Zhong-Qiang, and L. Ye-Dong, *J. Power Sources*, **34**, 141 (1991).